Journal of Power Sources 248 (2014) 852–860

Contents lists available at ScienceDirect

Journal of Power Sources

journal homepage: www.elsevier.com/locate/jpowsour

Stabilizing nanostructured lithium insertion materials *via* organic hybridization: A step forward towards high-power batteries

Dominic Bresser [a], Bernd Oschmann [b,c], Muhammad Nawaz Tahir [d], Wolfgang Tremel [d], Rudolf Zentel [b,*], Stefano Passerini [a,*]

[a] Institute of Physical Chemistry & MEET Battery Research Centre, University of Muenster, Corrensstrasse 28/30 & 46, 48149 Muenster, Germany
[b] Institute for Organic Chemistry, University of Mainz, Duesbergweg 10-14, 55128 Mainz, Germany
[c] Graduate School Materials Science in Mainz, Staudinger Weg 9, 55128 Mainz, Germany
[d] Institute for Inorganic and Analytical Chemistry, University of Mainz, Duesbergweg 10-14, 55128 Mainz, Germany

HIGHLIGHTS

- Structural disordering occurs in anatase TiO_2 nanorods (TiO_2 NRs) upon continuous cycling.
- Lowering the cathodic cut-off potential accelerates the structural disorder in TiO_2 NRs.
- Carbon coating prevents structural disordering upon cycling in TiO_2 nanorods.
- Dopamine is used as anchoring group for the RAFT polymerization derived carbon coating.
- Surface defects of TiO_2 NRs are healed by dopamine.

ARTICLE INFO

Article history:
Received 23 July 2013
Received in revised form
20 September 2013
Accepted 1 October 2013
Available online 16 October 2013

Keywords:
RAFT polymerization
Carbon coating
Anatase TiO_2 nanorods
Lithium-ion anode
Battery

ABSTRACT

Herein, we present the electrochemical characterization of carbon-coated TiO_2 nanorods, obtained by carbonizing RAFT (reversible addition fragmentation chain transfer) polymerization derived block co-polymers anchored on anatase TiO_2 nanorods. These carbon-coated TiO_2 nanorods show an improved electrochemical performance in terms of first cycle reversibility, specific capacity, cycling stability, and high rate capability. More importantly, however, the structural disordering observed in the uncoated TiO_2 nanorods by means of galvanostatic and potentiodynamic cycling as well as *ex situ* XRD analysis, does not occur for the carbon-coated material. Preventing this structural disordering does not only result in a stabilized cycling performance but, moreover, in substantially enhanced energy storage efficiency (86% *vs.* only 68% at the 100th cycle) due to the preserved characteristic potential profile of anatase TiO_2.

1. Introduction

Lithium-ion batteries are currently considered as one of the most promising electrochemical energy storage devices for future large-scale applications, as for instance electric vehicles [1–3]. However, beside improvements related to their energy density, current research activities focus on further advances of the obtainable power of such energy storage devices. In fact, the (dis-) charge capability of graphite, the state-of-the-art anode material is inherently limited by the release of the Li^+ solvation shell upon the intercalation of lithium ions through the initially formed solid electrolyte interphase (SEI) [4–6] as well as its very low operational potential and the concomitant safety issue of lithium plating [7,8]. Accordingly, alternative anode materials are investigated offering higher lithium ion (de-)insertion potentials and thus preventing the formation of an SEI layer as well as the risk of metallic lithium deposition at elevated charge/discharge rates. Titanium oxides, as for instance $Li_4Ti_5O_{12}$ (LTO) or different polymorphs of TiO_2, have gathered a wide interest [9–16] since such materials offer decent specific capacities, due to their higher density with respect to graphite, and lithium (de-)insertion occurs at potentials within the electrochemical stability window of commonly used organic carbonate-based electrolytes. While LTO is already comprised in

* Corresponding authors.
E-mail addresses: zentel@uni-mainz.de (R. Zentel), stefano.passerini@uni-muenster.de (S. Passerini).

0378-7753/$ – see front matter © 2013 Elsevier B.V. All rights reserved.
http://dx.doi.org/10.1016/j.jpowsour.2013.10.013

commercial lithium-ion batteries [2], anatase TiO_2 is certainly a very attractive alternative due to its natural abundance, its already available large-scale production, such as pigments for the paint industry and dye-sensitized solar cells [17–19], as well as its theoretically higher specific capacity (335 mAh g^{-1} *vs.* 175 mAh g^{-1} for LTO). However, micro-sized anatase TiO_2 severely suffers of limited specific capacities especially at high rates [20–22]. Nanostructuring of such active material particles showed substantial improvements in terms of achievable specific capacity, due to the increasing capacity contribution resulting from a second phase formation, which occurs only at the particle surface [23–26]. The high rate capability is also improved by an increasing solid solution domain [24–27], a generally reduced lithium ion and electron diffusion and transport pathways and an increased electrode/electrolyte contact area [28,29]. Further improvement was achieved by embedding such nanoparticles in carbonaceous host matrices or applying a carbon coating layer in order to enhance the electronic conductivity of such mostly insulating active material [30]. Wang et al. [31], for instance, investigated self-assembled TiO_2-graphene hybrid nanostructures, showing enhanced rate performance, *i.e.*, more than 100 mAh g^{-1} at C rates as high as 30C. Fu et al. [32], Das et al. [33], or Cao et al. [34] followed a rather facile approach using sucrose or glucose as carbon precursor, while Thackeray and co-workers [35] reported an *in situ* carbon coating procedure utilizing titanium (IV) oxyacetyl acetonate as TiO_2 and carbon precursor and a specially designed autogenic reactor. Using the oleic acid capping agent to form a carbonaceous coating layer on TiO_2 nanorods, Bresser et al. [26] obtained an advanced rate performance, particularly when only the charge (delithiation) rate was increased, and high specific capacities of more than 250 mAh g^{-1}, depending on the cathodic cut-off potential. However, it appears noteworthy that this list of anatase TiO_2-carbon heterogeneous secondary structures presents only a brief overview on previously reported work and is certainly not exhaustive. Generally, for active materials storing lithium ions by insertion mechanism, as *inter alia* anatase TiO_2, thus undergoing relatively low volume changes upon reversible lithium uptake, homogenous and rather thin coating layers are preferable. This allows an improved electron transport, while at the same time lithium ion diffusion into the active material particles is not slowed down [36], thus resulting in an improved high rate capability of such electrode materials [37]. Very recently, we reported a new approach for the realization of such a carbon coating based on the carbonization of a block copolymer anchored onto the nanoparticles surface and synthesized by RAFT (reversible addition fragmentation chain transfer) polymerization (Fig. 1), showing an improved cycling stability and reduced capacity fading per cycle relatively to the uncoated TiO_2 nanorods [38].

Herein, we will present a detailed and extended electrochemical characterization of these carbon-coated anatase TiO_2 nanorods, showing their advanced high rate capability, specific capacity, cycling stability, and first cycle reversibility relatively to the uncoated TiO_2 nanorods. Even more remarkably, however, it will be shown that the application of such a carbon coating suppresses a continuously progressing structural disorder observed in uncoated anatase nanorods by means of galvanostatic and potentiodynamic cycling as well as *ex situ* XRD analysis of cycled electrodes. This structural disordering does not only result in inferior capacity retention but moreover in a substantially reduced energy storage efficiency caused by continuous shortening of the characteristic potential plateau upon lithium (de-)insertion, which is – to the best of our knowledge – herein investigated and discussed for the first time.

2. Experimental section

2.1. Synthesis of carbon-coated and uncoated anatase TiO_2 nanorods

The synthesis of carbon-coated and uncoated anatase TiO_2 nanorods was very recently described in detail by Oschmann et al. [38]. In brief, oleic acid (OLEA, Acros Organics)/oleylamine (OAM, Acros Organics) – capped anatase TiO_2 nanorods were synthesized according to a solvothermal method recently reported by Dinh et al. [39], using titanium butoxide (Acros Organics) as precursor and water vapor as hydrolysis agent. OLEA and OAM were subsequently replaced by tetrafluoroborate (BF_4^-), using nitrosonium tetrafluoroborate ($NOBF_4$, Sigma–Aldrich) in dichloromethane solution, according to a ligand-exchange reaction reported by Dong et al. [40]. For the preparation of reference electrodes based on uncoated TiO_2 nanorods, BF_4^- was removed by means of centrifugation and dialysis in methanol. For the preparation of carbon-coated TiO_2 nanorods, the BF_4^--capped nanorods were dispersed in *N*,*N*-dimethylformamide (DMF) and mixed with the RAFT (reversible addition fragmentation chain transfer) polymerization-derived block copolymer poly(acrylonitrile-b-dopamine acrylamide) (P(AN-b-DAAM)), comprising polyacrylonitrile (PAN) as carbon precursor and dopamine as anchor block. The polymer to TiO_2 ratio was 1:4. Subsequently, the block copolymer-functionalized TiO_2 nanorods were purified *via* centrifugation and dried under vacuum. For the carbonization of the block copolymer, the functionalized nanorods were thermally treated under argon (for 240 min at 300 °C & for 90 min at 700 °C; heating rate: 5 °C min^{-1}).

2.2. Morphological and structural characterization

The structure of uncoated and carbon-coated anatase TiO_2 nanorods was investigated by means of X-ray diffraction (XRD) analysis using a Siemens D5000 (Cu-Kα radiation, $\lambda = 0.154$ nm). Raman spectroscopy was performed by means of a Horiba Jobin Y

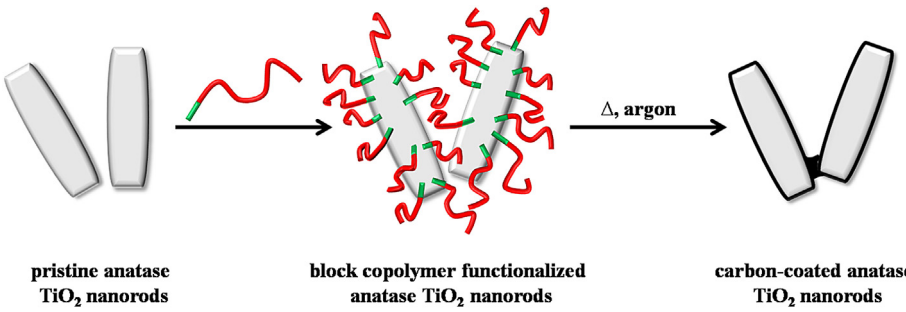

Fig. 1. Schematic illustration of the carbon coating approach: as-synthesized TiO_2 nanorods (left) are functionalized by grafting a block copolymer (center), which is subsequently carbonized by a thermal treatment at 300 °C for 4 h and at 700 °C for 1.5 h under argon, resulting in a thin and homogenous carbon coating (right).

LabRAM HR Spectrometer, equipped with a frequency doubled Nd:YAG laser. Transmission electron microscopy (TEM) and high resolution transmission electron microscopy (HRTEM) analysis of carbon-coated and uncoated TiO_2 nanorods was conducted using a Tecnai F30 ST FEI. For TEM and HRTEM analysis, the studied samples were dispersed on a non-porous, carbon-free silicon-based sample holder. *Ex situ* XRD analysis of galvanostatically and potentiodynamically cycled electrodes was carried out using a Bruker D8 Advance (Cu-Kα radiation, $\lambda = 0.154$ nm). The patterns were aligned according to the major (101) reflection of anatase TiO_2.

2.3. Electrochemical characterization

Electrodes based on carbon-coated anatase TiO_2 (and for comparison reasons, uncoated TiO_2) nanorods were prepared according the following procedure: Sodium carboxymethyl cellulose (CMC, Walocel CRT 2000PA, Dow Wolff Cellulosics) was dissolved in deionized water (1.25 wt.%). Subsequently, the carbon-coated (and uncoated) TiO_2 nanorods and Super C65® were added. The resulting mixture was homogenized by means of a planetary ball mill (Vario-Planetary Mill Pulverisette 4, FRITSCH) for 2 h set at 800 rpm. The obtained electrode paste was coated on dendritic copper foil (SCHLENK) with a wet film thickness of 130 μm and dried at ambient temperature for around 12 h. Disc electrodes with a diameter of 12 mm were punched and dried for about 24 h at 120 °C under vacuum. The content of active material on the disc electrodes was in a range of 1.6–2.0 mg cm^{-2} for carbon-coated TiO_2 and in a range of 1.7–2.1 mg cm^{-2} for uncoated TiO_2 nanorods. Electrodes based on carbon-coated TiO_2 nanorods had a final composition of 75 wt.% of TiO_2, 5 wt.% of CMC, and 20 wt.% of carbon (5 wt.% of Super C65® resulting from the previous processing, 10 wt.% of carbon coating as confirmed by TGA under O_2, and 5 wt.% of Super C65® added later upon the preparation of the electrodes). Reference electrodes based on uncoated TiO_2 nanorods were prepared replacing the carbon content of the coating layer by additional Super C65®, which was added upon the electrode preparation. Swagelok™-type cells were assembled in an MBraun glove box with an O_2 and H_2O content of less than 0.5 ppm. Polypropylene fleeces (Freudenberg FS2190), drenched with the utilized electrolyte (1 M $LiPF_6$ in a 3:7 volume mixture of ethylene carbonate and diethyl carbonate, UBE) were used as separator. Since lithium foil (Rockwood Lithium, battery grade) was used as counter and reference electrodes, all potential values given in this manuscript refer to the Li/Li^+ reference couple. Galvanostatic cycling was carried out by means of a Maccor Battery Tester 4300. An applied C rate of 1C corresponds to an applied specific current of 168 mA g^{-1}, considering $x = 0.5$ as the reference limit for the insertion reaction: $TiO_2 + x(Li^+ + e^-) \rightarrow Li_xTiO_2$. Cyclic voltammetry was performed utilizing a VMP3 potentiostat (BioLogic), applying a scan rate of 0.1 mV s^{-1}.

3. Results and discussion

3.1. Morphological and structural characterization

In a first step, both samples – uncoated and carbon-coated TiO_2 nanorods – were investigated by means of XRD in order to confirm the preservation of the anatase structure (Fig. 2). Indeed, both patterns show only reflections corresponding to the anatase phase (ICSD 172914) having the space group $I4_1/amd$. No additional reflections indicating phase impurities can be observed. Accordingly, the sample does not undergo a phase change to the principally more stable rutile phase [41,42] upon the thermally induced carbonization of the surface-anchored, RAFT polymerization-derived block copolymer. This is in good agreement with earlier reported results on anatase TiO_2 nanorods [26,43], indicating the enhanced stability of the anatase phase relatively to the rutile phase for nano-sized particles due to the increasing impact of the surface free energy, which is lower for the anatase phase compared to the rutile phase, on the total free energy with decreasing particle size [41,42,44].

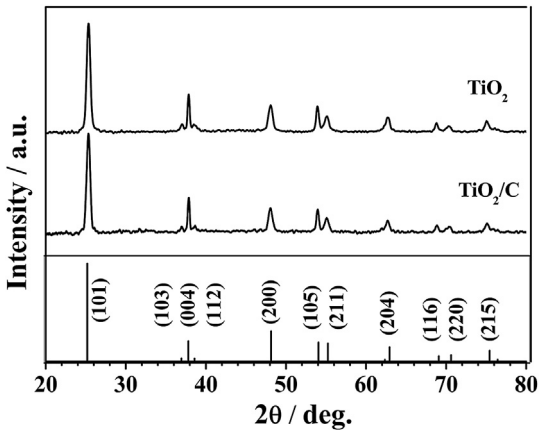

Fig. 2. XRD patterns of uncoated anatase TiO_2 nanorods (TiO_2, upper pattern) and after thermal treatment applied in order to carbonize the grafted copolymer (TiO_2/C, lower pattern). The reference ICSD 172914 for anatase TiO_2 is given in the bottom.

The formation of a very thin (approximately 1 nm) and amorphous surface film on the TiO_2 nanorods, having an average length of around 30 nm and an average diameter of about 10–15 nm (Fig. 3a), was confirmed by HRTEM analysis of uncoated (Fig. 3b) and carbon-coated (Fig. 3c) TiO_2 nanorods. In fact, this coating layer is covering the nanorods surface very homogenously. Slight accumulation of carbon is observed only at the boundary of adjacent nanorods (Fig. 3c), as also schematically illustrated in Fig. 1. Such a carbonaceous conductive "bridge", however, might have a beneficial effect on the electrochemical performance of the sample, enabling a fast electron transfer from one particle to another and finally to the current collector.

For a further characterization of the carbon coating, Raman spectroscopy was carried out (Fig. 4). While for the copolymer-functionalized TiO_2 sample (*i.e.*, prior to the thermally induced carbonization of the grafted polymer; gray dashed spectrum in Fig. 4a) the characteristic Raman bands for anatase TiO_2 [45] are clearly observed, their intensity is significantly decreased for the carbon-coated sample (*i.e.*, after the thermal treatment; black spectrum in Fig. 4a), being in good agreement with previously reported results [26]. In addition, the characteristic G and D bands, appearing at around 1580 and 1355 cm^{-1} and corresponding to the graphitic C–C stretching and induced disorder of sp^2 hybridized carbon [46,47], respectively, are observed only for the carbon-coated sample, confirming the presence of a partially graphitic carbonaceous surface layer on the anatase TiO_2 nanorods (Fig. 4b).

3.2. Electrochemical characterization

For the electrochemical characterization of carbon-coated and uncoated TiO_2 nanorods, electrodes were prepared using carboxymethyl cellulose (CMC) as binder, since it was shown that electrodes comprising CMC rather than polyvinylidene fluoride (PVdF) present an improved electrochemical performance [48,49]. Moreover, it appears noteworthy that for the preparation of carbon-coated TiO_2-based electrodes, the conductive carbon (Super C65®) was added partially before and after the thermal treatment,

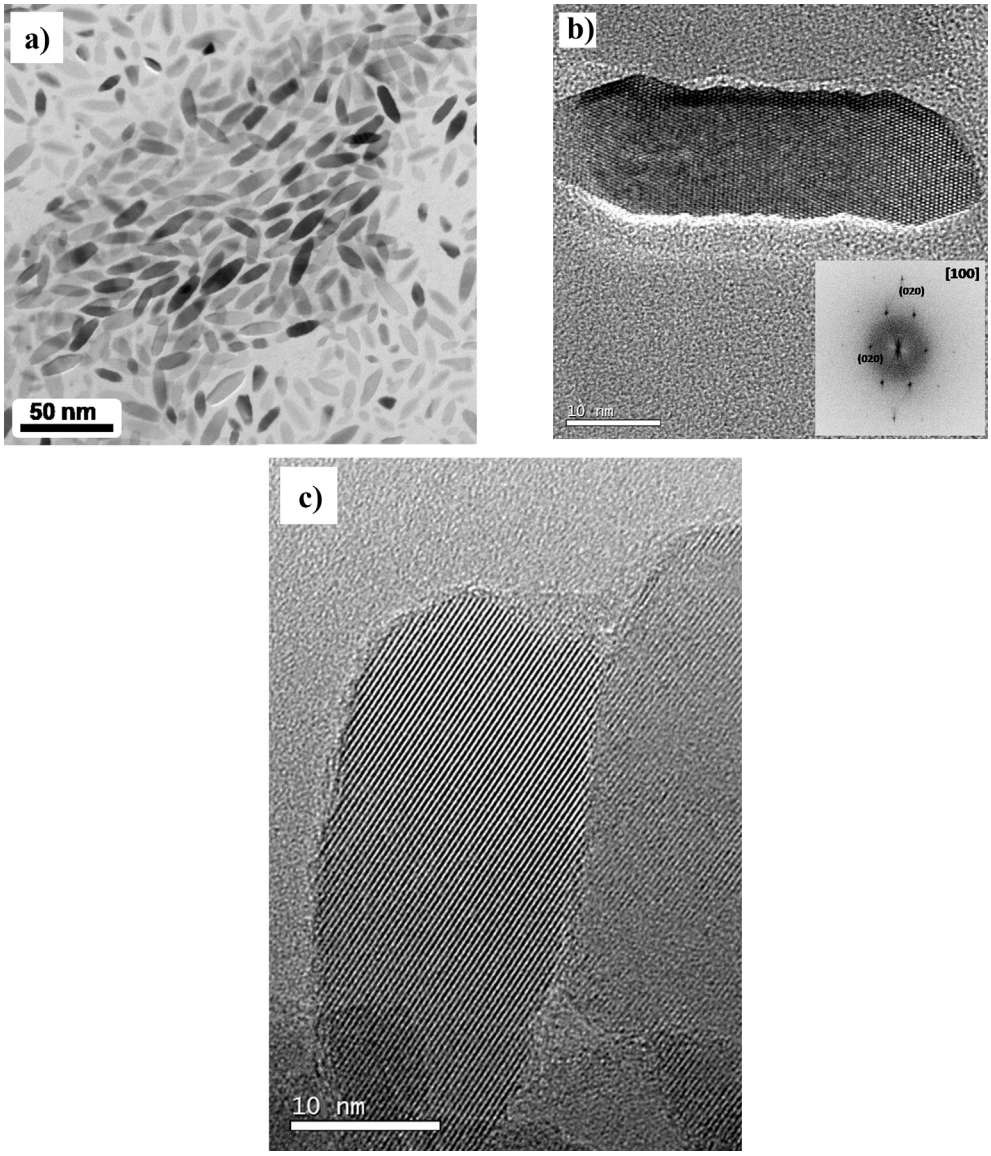

Fig. 3. TEM and HRTEM images of uncoated (a and b) TiO_2 nanorods. Inset in b): the Fast Fourier Transform (FFT) showing the [100] direction of anatase TiO_2. c) HRTEM image of carbon-coated TiO_2 nanorods after thermal carbonization of the grafted block copolymer.

following a previously reported electrode material processing [26]. Generally, however, electrodes based on carbon-coated TiO_2 nanorods will be hereinafter referred to as TiO_2/C while those based on uncoated TiO_2 nanorods will be simply referred to as TiO_2.

In Fig. 5, a comparison of the high rate capability for TiO_2/C and TiO_2 is presented. As expected, TiO_2/C-based electrodes show a significantly improved rate capability. Specific capacities of around 220, 190, 170, and 135 mAh g^{-1} were obtained for TiO_2/C at 0.2C, 1C, 2C, and 5C, respectively, while TiO_2-based electrodes delivered specific capacities of 10–20 mAh g^{-1} lower for all C rates (see also Table 1). More importantly, the cycling stability was dramatically improved as revealed by the lower specific capacity decrease upon continuous cycling at all C rates, and particularly at 1C for the subsequent constant current cycling, evidencing the highly reversible lithium (de-)insertion for carbon-coated TiO_2 nanorods. As a matter of fact, the coulombic efficiency for TiO_2/C approaches 99.97% upon continuous cycling at 1C, while the efficiency for TiO_2 remains comparably low at about 99.7%.

A more careful analysis of the obtained data performed by plotting the potential *vs.* the specific capacity (Fig. 6) reveals that the first (dis-)charge profile for carbon-coated (Fig. 6a) as well as for uncoated (Fig. 6b) nanorods shows the characteristic potential profile for nanostructured anatase TiO_2 [20,25,26,50–52]. Upon the initial rather smooth voltage decrease lithium ions are inserted *via* solid solution into the Li-poor phase of anatase TiO_2 up to a lithiation degree of around $Li_{0.1}TiO_2$ ($\approx$33 mAh g^{-1}) for carbon-coated TiO_2 (TiO_2/C, Fig. 6a), while retaining the $I4_1/amd$ space group and its tetragonal symmetry. The subsequent distinct potential plateau at around 1.7 V corresponds to the occurring phase transition and co-existence of the Li-rich $Li_{0.5}TiO_2$ ($\approx$168 mAh g^{-1}, Fig. 6a) phase, having a lithium titanate structure and orthorhombic symmetry (space group: *Imma*). Finally, the second phase change, occurring only at the nanoparticles surface [24,53–55], from Li-rich lithium titanate back to the anatase phase ($LiTiO_2$, space group $I4_1/amd$) is taking place, as indicated by the following voltage plateau at around 1.5 V [26,54,55]. This results in a total lithiation of the active material up to $Li_{0.77}TiO_2$ (Fig. 6a, TiO_2/C). It should be mentioned

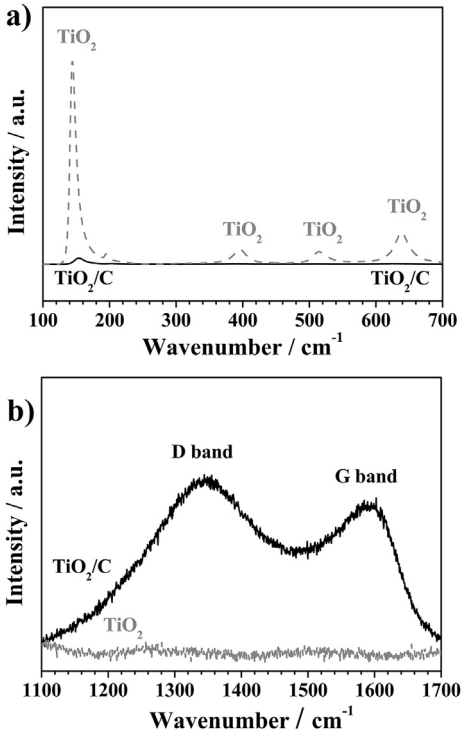

Fig. 4. Raman spectra comparing block copolymer-functionalized (gray, dashed line) and carbon-coated (black) anatase TiO_2 nanorods. a) Comparison of the lower wavenumber region for the bands related to anatase TiO_2. b) Comparison of the higher wavenumber region for the bands corresponding to the carbonaceous coating.

here, that other studies have assigned the presence of the second voltage plateau to a kinetically hampered, ongoing lithium insertion in orthorhombic TiO_2 [56], while the increased capacity values for nanostructured materials would be caused by (pseudo-)capacitive lithium storage [56,57]. In fact, within scientific literature it is still under discussion whether the second phase transition is taking place for nanostructured anatase TiO_2 in an electrochemical cell. However, based on the results presented herein, we cannot ultimately exclude one explanation or the other. Actually, both phenomena (second phase transition and (pseudo-)capacitive lithium storage) might contribute to the obtained specific capacities.

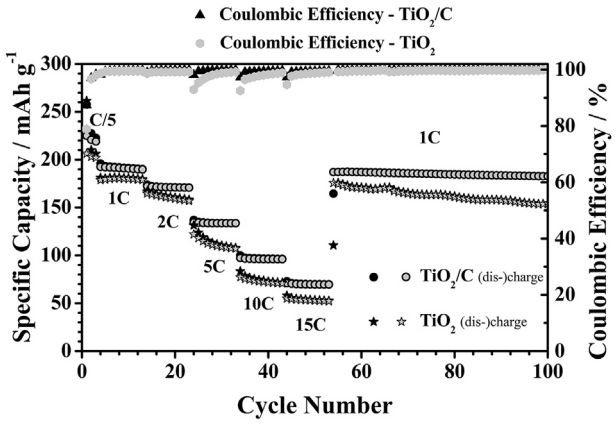

Fig. 5. Carbon-coated and uncoated TiO_2 nanorods-based electrodes subjected to galvanostatic cycling at elevated C rates (cycles 1–3 at C/5, followed by each 10 cycles at 1C, 2C, 5C, 10C, and 15C, finally (dis-)charged at 1C again); cut-off potentials: 1.2 and 3.0 V.

Table 1
Reversible specific capacity for TiO_2/C- and TiO_2-based electrodes at different C rates and the corresponding cycle number.

Cycle number	C rate (1C = 168 mA g^{-1})	Specific capacity (TiO_2/C)/mAh g^{-1}	Specific capacity (TiO_2)/mAh g^{-1}
2	C/5	221	203
10	1C	191	180
20	2C	171	159
30	5C	134	109
40	10C	96	72
50	15C	70	53
55	1C	187	174
100	1C	183	154

However, while for the carbon-coated sample a reversible specific capacity of 225 mAh g^{-1} and a coulombic efficiency of 87.4% are obtained, the uncoated sample delivers a reversible capacity of only 206 mAh g^{-1} and a coulombic efficiency of 78.9%. This improved first cycle efficiency of TiO_2/C might be related to a reduced surface activity due to the thin carbon layer and thus a decrease of the amount of parasitic surface reactions, *inter alia* caused by reductive electrolyte decomposition [26]. In addition, the initial lithium trapping inside the TiO_2 host [58] might be reduced due to the enhanced electronic conductivity and thus kinetics of TiO_2/C relatively to TiO_2. In fact, the specific capacity obtained reversibly upon delithiation (charge) up to the appearance of the voltage plateau is higher for TiO_2/C (≈68 mAh g^{-1}) than for TiO_2 (≈55 mAh g^{-1}), indicating an increased contribution of the second phase change from anatase back to titanate. The subsequent slight overvoltage at the onset of the potential plateau (titanate → anatase) appears to be correlated to the primary particle size of the anatase TiO_2 nanoparticles and has been assigned to a nucleation barrier for the initiation of a phase transition [20,59–61].

Selected potential profiles for the different C rates (Fig. 6c and d) show once again the enhanced rate capability and capacity retention after the rate tests of TiO_2/C. Moreover, it is observed that the second phase change, indicated by the second voltage plateau at around 1.5 V appears only for lower (dis-)charge rates, up to 1C, due to kinetic limitations [26,55]. Additionally, however, the potential profile corresponding to cycle 55 for TiO_2 (second profile at 1C, Fig. 6d) presents a new feature at a potential of around 2.8 V. This phenomenon becomes even more obvious by comparing the potential profiles at 1C only up to the 100th cycle (Fig. 6e and f). Indeed, while TiO_2/C presents a stable cycling and only a slight capacity loss caused by a slight shortening of the main voltage plateau (Fig. 6e), TiO_2 presents a more dramatic change of the potential profile upon continuous (de-)lithiation (Fig. 6f). The main voltage plateaus observed around 1.7 and 1.9 V during the discharge (lithiation) and charge (delithiation), respectively, are continuously shrinking (Fig. 6f). Upon 100 cycles the lithium insertion was mainly taking place at lower potentials (in average at around 1.5 V) while a new voltage plateau at about 2.8 V appeared for the delithiation process, accompanied by a shift of the overvoltage at the onset of the main potential plateau to higher voltages (indicated by the red arrow in web version). It is extremely important to notice that a potential relaxation is observed when a TiO_2-based electrode upon delithiation at 2.8 V is left in open circuit conditions (results not shown). In particular, upon relaxation (a few hours) the potential drops to around 2.0 V thus indicating the kinetic origin of the high voltage delithiation plateau. However, such a modification of the lithium (de-)insertion process results in a dramatically reduced energy storage efficiency of uncoated TiO_2 nanoparticles (Fig. 7). A similar behavior was, in fact, already observed by Saravanan et al. [62]. Unfortunately, within their study this phenomenon was neither described nor discussed.

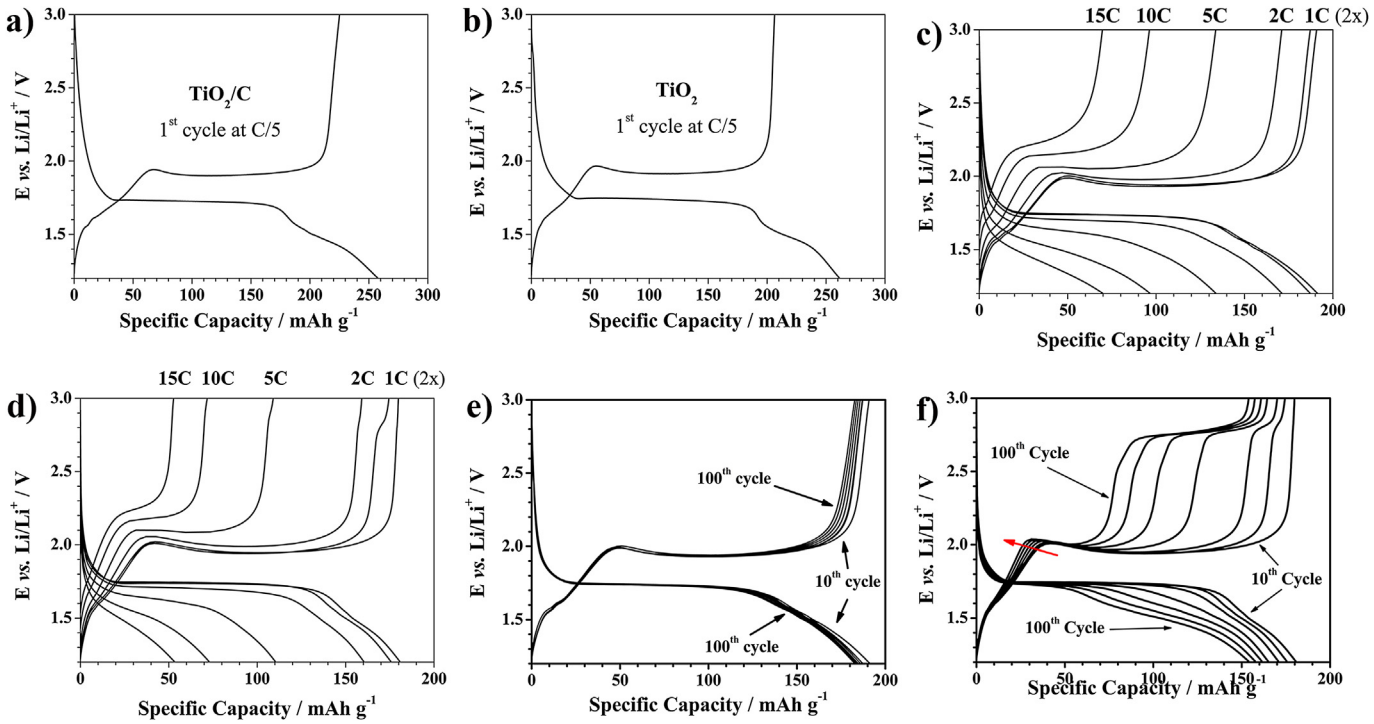

Fig. 6. Potential profile of the first galvanostatic cycle (see Fig. 5) for carbon-coated (a) and uncoated (b) anatase TiO_2 nanorods at C/5 (~33.6 mA g^{-1}). Selected potential profiles for carbon-coated (c) and uncoated (d) TiO_2 nanorods at elevated C rates (1C, 2C, 5C, 10C, 15C, and 1C again). Selected potential profiles at a constant C rate of 1C for carbon-coated (e) and uncoated (f) TiO_2 nanorods. Cut-off potentials: 1.2 and 3.0 V.

In order to further investigate this phenomenon, cyclic voltammetry was performed on non-coated TiO_2-based electrodes for 50 continuous cyclic sweeps (Fig. 8). Initially, the expected cyclic voltammogram is observed, indicating the two redox couples for the first and second phase transition [26]. Two very minor anodic and cathodic peaks at voltages of around 1.5 and 1.6 V have already been observed in literature and assigned to a reversible pseudo-capacitive effect [63] and indeed they are highly reversible even after 50 continuous potentiodynamic sweeps. Kavan and co-workers have very recently reported the electrochemical characterization of TiO_2 (B) and anatase TiO_2 as well as their mixtures, investigating the capacitive contribution for these two titanium oxide phases to the overall lithium storage [64]. According to their results obtained by cyclic voltammetry, particularly with respect to the mixture of anatase TiO_2 and TiO_2 (B), these two peaks might also be related to the presence of a very minor impurity of TiO_2 (B), for which, as a matter of fact, the (pseudo-)capacitive lithium storage plays a decisive role [65]. Due to an overlap of the major XRD reflections [66], the presence of a very minor amount of TiO_2 (B) within the herein studied anatase TiO_2 nanorods cannot be fully ruled out, particularly if the relative amount is below the XRD detection limit. However, Raman spectroscopy did not reveal the presence of TiO_2 (B), apart from an extremely weak peak at about 200 cm^{-1} (Fig. 4a). In order to verify the presence of TiO_2 (B) impurities, a more careful structural analysis of the sample would have to be performed, which is beyond the scope of this manuscript.

More remarkably, however, is the appearance of a new redox couple at around 1.5–1.35 V and 2.6–2.7 V for the cathodic and anodic sweep, respectively. While these peaks are increasing, the main redox couple is decreasing in terms of specific current (indicated by the black arrows), being perfectly in line with the former results obtained by galvanostatic cycling (Fig. 6d and f). In fact, to the best of our knowledge such a newly appearing redox couple has

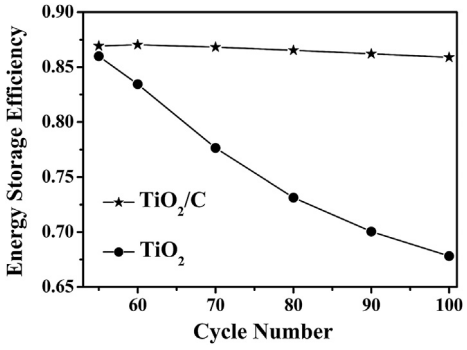

Fig. 7. Comparison of the energy storage efficiency for TiO_2/C and TiO_2 (~ratio of energy stored upon charge *vs.* energy released upon discharge according to the theoretically reversed process of charge and discharge in a lithium-ion full-cell within which the TiO_2-based electrode would serve as anode).

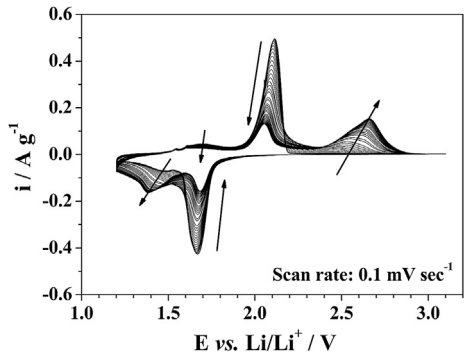

Fig. 8. Cyclic voltammogram of an uncoated TiO_2 nanorods-based electrode (TiO_2) from the 5th to the 50th cyclic sweep; reversing potentials: 1.2 and 3.0 V.

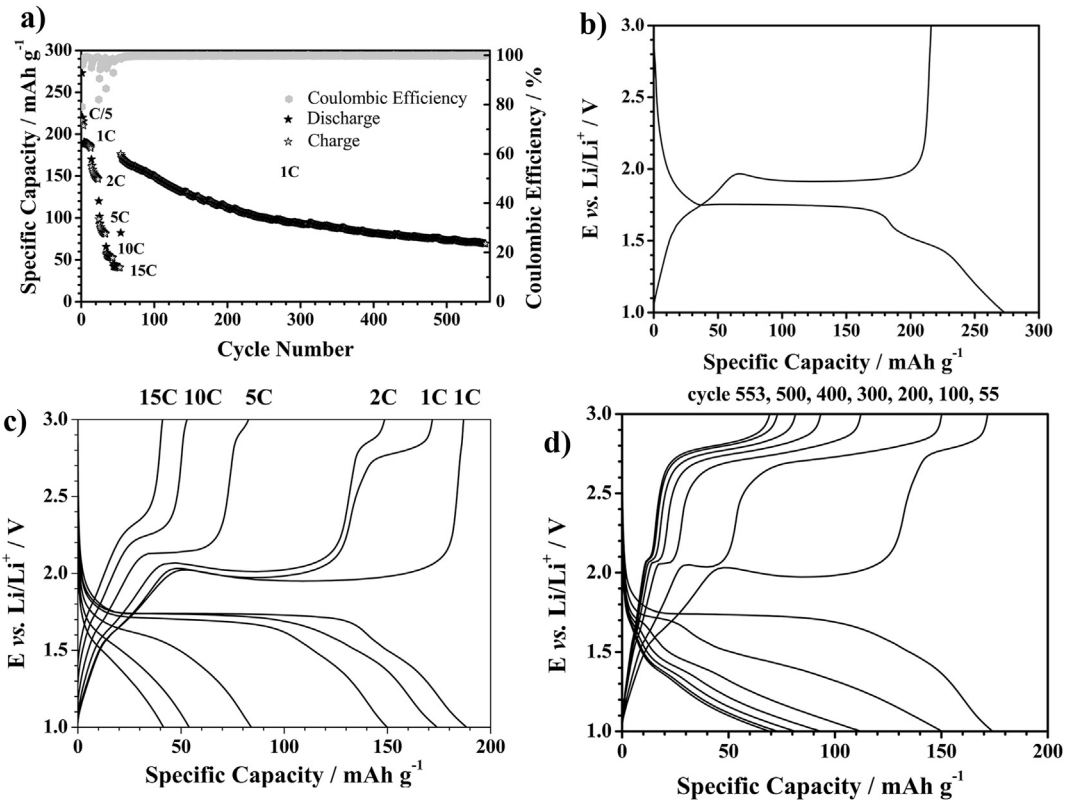

Fig. 9. Performance of uncoated TiO_2 nanorod electrode subjected to galvanostatic cycling at elevated C rates (cycles 1–3 at C/5, followed by each ten cycles at 1C, 2C, 5C, 10C, and 15C, finally (dis-)charged at 1C for all subsequent cycles (cut-off potentials: 1.0 and 3.0 V) (panel a)). b) Corresponding potential profile for the 1st cycle. c) Selected potential profiles for elevated C rates (1C, 2C, 5C, 10C, 15C, and 1C again). d) Selected potential profiles for the subsequent cycling at 1C.

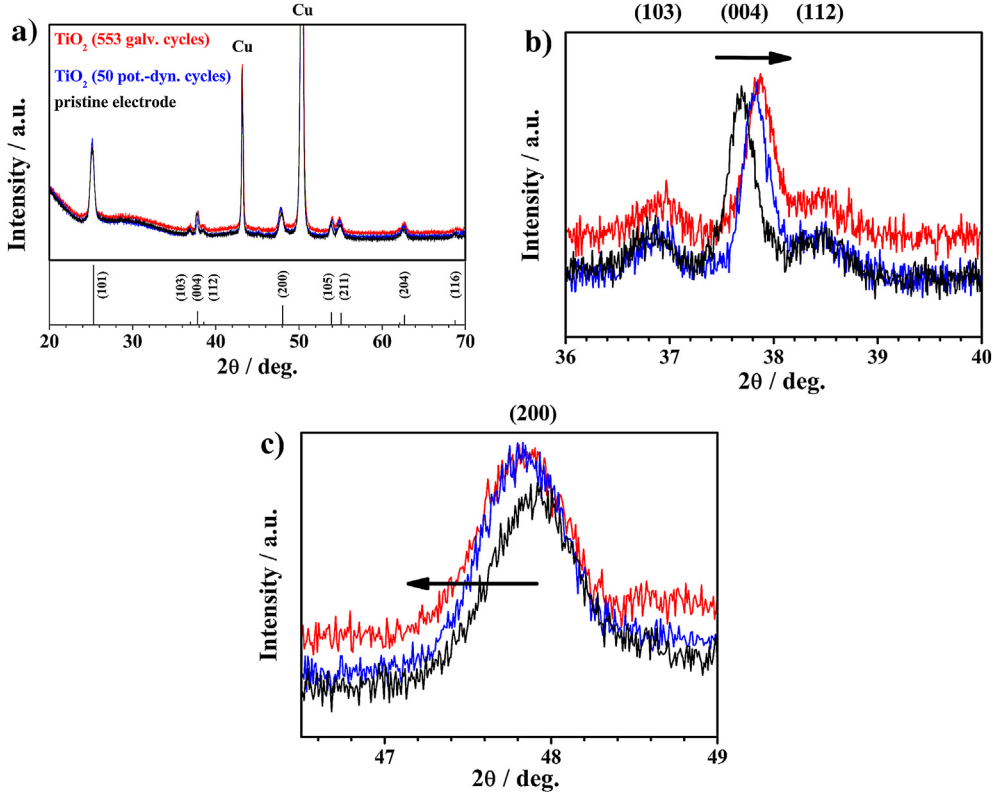

Fig. 10. Comparative *ex situ* XRD investigation of pristine (black pattern), galvanostatically (red pattern, cut-off potentials: 1.0 and 3.0 V, Fig. 9), and potentiodynamically (blue pattern, reversing potentials: 1.2 and 3.0 V, Fig. 8) cycled electrodes based on uncoated anatase TiO_2 nanorods (a). The reference for anatase TiO_2 (ICSD 172914) is given in the bottom. b) and c) show magnifications of the (004) and (200) reflections, respectively. (For interpretation of the references to color in this figure legend, the reader is referred to the web version of this article.)

never been reported so far for anatase TiO_2. For a further investigation of this phenomenon *ex situ* XRD analysis of the cycled electrodes was carried out (see later in Section 3.3).

As it has been shown that the lower cut-off potential has a significant influence on the electrochemical performance of anatase nanoparticles [26], we studied also the influence of the cut-off potential on the appearance of this new potential profile feature, occurring for uncoated TiO_2 nanorods only (Fig. 9). Generally, the previously reported results [26] were confirmed: lowering the cathodic cut-off potential from 1.2 V to 1.0 V resulted in a slightly increased reversible specific capacity in the first cycle (216 *vs.* 206 mAh g^{-1}; Fig. 9a and b) and for rather low specific currents (187 *vs.* 180 mAh g^{-1} at 1C in the 10th cycle). However, at higher C rates the situation is reversed (149 *vs.* 159 mAh g^{-1} at 2C; 83 *vs.* 109 mAh g^{-1} at 5C; 53 *vs.* 72 mAh g^{-1} at 10C; 41 *vs.* 53 mAh g^{-1} at 15C; see also Table 1 for the values for 1.2 V as cut-off potential). In fact, by setting the C rate back to 1C similar capacity values are obtained for both cut-off potentials (171 *vs.* 174 mAh g^{-1} and 150 *vs.* 154 mAh g^{-1} for the 55th and 100th cycle and 1.0 *vs.* 1.2 V as cathodic cut-off potential, respectively), indicating a more pronounced capacity fading for the lower cut-off potential (Fig. 9a). A comparison of the potential profiles at elevated C rates (Figs. 9c and 6d), however, reveals that the lower cut-off potential has also an influence on the appearance of the new plateau-like feature at higher potentials of around 2.8 V. It is obvious that this feature appears much earlier for a cut-off potential of 1.0 V, even for elevated rates of 2C and 5C, while it is at the same time much more pronounced for the 55th cycle (1C again). In fact, subjecting a TiO_2-based electrode to more than 550 (dis-)charge cycles confirms that the lengthening of the new plateau-like feature at the expense of shortening of the main voltage plateau is a continuous process (Fig. 9d). Almost no capacity is obtained anymore along the main voltage plateau, while the major contribution stems from the lithium deinsertion at potentials at around 2.8 V.

3.3. *Ex situ XRD analysis*

A continuous change of the TiO_2 phase away from anatase towards a new crystalline structure might explain the observed new redox couple (Fig. 8) and the occurrence of a new voltage plateau (Figs. 6f and 9d). Preliminary investigation of cycled electrodes by means of *ex situ* XRD, however, revealed a preservation of the anatase phase of uncoated TiO_2 nanorods even after extended galvanostatic cycling (Fig. 10a). Nevertheless, a more careful analysis of the obtained XRD patterns revealed that the reflections for the (004) (Fig. 10b) and the (200) plane (Fig. 10c) appear to be slightly shifted to higher and lower 2θ values indicating a slight reduction and expansion of the lattice along the [001] and [100] direction, respectively. These findings are, in fact, in good agreement with an earlier report by Rabatic et al. [67], who identified an expansion of the anatase lattice along the [100] direction for the surface layer of TiO_2 nanorods, and particularly at the tips of ellipsoid nanoparticles. Indeed, HRTEM images of uncoated anatase TiO_2 nanorods indicate less sharp particle edges at the tip of the rods, leading to the suggestion that particle growth did not reach equilibrium, yet, and thus might be more affected by such kind of surface defects (Fig. 11).

Besides, it is agreed in scientific literature that lithium (de-) insertion in anatase TiO_2 occurs preferably along the [001] direction (*i.e.*, along the *c*-axis) [68,69], meaning that a decrease of the lattice parameter along this direction would result in a kinetic hindrance of lithium diffusion into and within the lattice [68,70], which is in line with the observed shift of the lithium insertion and deinsertion towards lower and higher potentials, respectively, and the previously mentioned relaxation of the open circuit voltage upon rest.

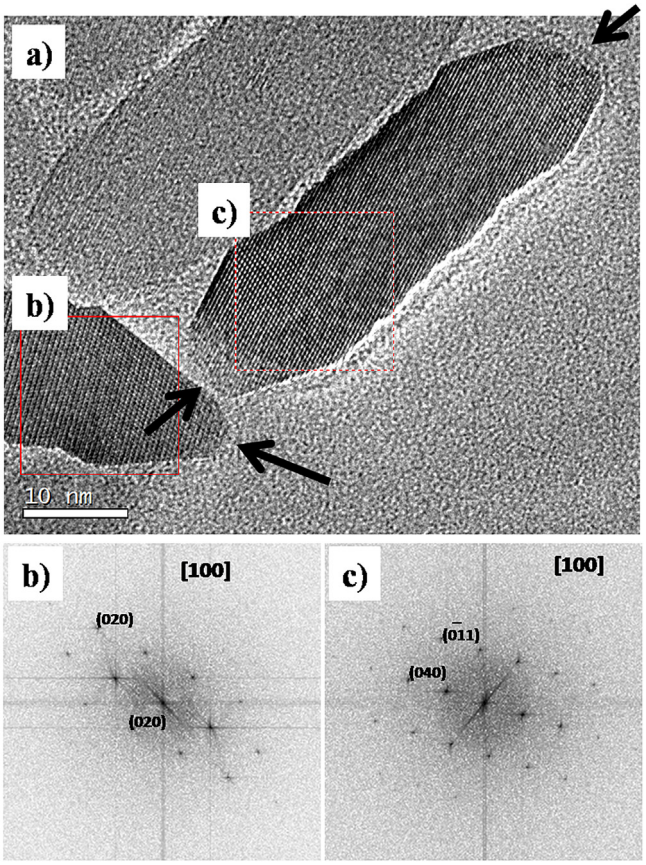

Fig. 11. HRTEM image of uncoated anatase TiO_2 nanorods (a). b) and c) show the Fast Fourier Transforms (FFT) for the two nanorods in panel a. The black arrows point on the tip of these nanorods, indicating the crystal growth along the [100] direction.

Moreover, according to the electrochemical results this structural disordering appears to be a continuously progressing phenomenon upon ongoing lithium ion (de-)insertion – presumably starting from the particle surface and proceeding towards the particle core.

Interestingly, Rabatic et al. reported that the lattice distortion in TiO_2 nanorods could be healed by a controlled reaction with dopamine [67], which has been used in the present work as anchor group within the RAFT polymerization as intermediate step upon the carbon coating process. Indeed, *ex situ* XRD analysis of electrodes based on carbon-coated TiO_2 nanorods does not present any shift of the (200) reflection after about 50 galvanostatic (dis-) charge cycles (results not shown herein) being in good agreement with the results reported by Rabatic et al. [67]. This allows us to suggest that the carbon coating process (including the thermal treatment) might play a fundamental role in preventing the structural disordering for carbon-coated TiO_2 nanorods, thus granting their exceptional long-term electrochemical performance.

4. Conclusions

The effect of a carbon coating process based on the carbonization of PAN-based block copolymers anchored onto anatase TiO_2 nanorods on their performance was presented. This carbon coating process resulted in the formation of a homogenous and thin carbonaceous layer on the TiO_2 nanorods surface. Thus carbon-coated TiO_2 nanorods showed a significantly enhanced electrochemical performance in terms of high rate capability, coulombic efficiency, and cycling stability. More remarkably, the application of the carbon coating prevented the appearance of an up to today

never discussed alteration of the lithium ion (de-)insertion mechanism of anatase TiO_2 caused by the occurrence of a structural disorder upon continuous lithium storage and release. This structural disordering led to a continuously changing potential profile and the appearance of a new redox couple in the cyclic voltammogram of such electrodes, which finally resulted not only in a less stable cycling performance but moreover in a dramatically reduced energy storage efficiency of such electrodes.

Acknowledgments

D.B. and S. P. would like to thank the European Commission for financial support within the ORION (229036) and the AMELIE (265910) project under the Seventh Framework Programme (7th FWP). B.O. would like to acknowledge financial support by the "Fonds der Chemischen Industrie". Furthermore, the authors would like to thank Dr. U. Kolb and R. Branscheid for performing HRTEM analysis.

References

[1] M. Armand, J.-M. Tarascon, Nature 451 (2008) 652.
[2] B. Scrosati, J. Garche, J. Power Sources 195 (2010) 2419.
[3] B. Scrosati, J. Hassoun, Y.-K. Sun, Energy Environ. Sci. 4 (2011) 3287.
[4] T. Abe, H. Fukuda, Y. Iriyama, Z. Ogumi, J. Electrochem. Soc. 151 (2004) A1120.
[5] Y. Yamada, Y. Iriyama, T. Abe, Z. Ogumi, Langmuir 25 (2009) 12766.
[6] E. Peled, J. Electrochem. Soc. 126 (1979) 2047.
[7] R. Yazami, Electrochim. Acta 45 (1999) 87.
[8] S. Flandrois, B. Simon, Carbon – Am. Carbon Commun. 37 (1999) 165.
[9] Z. Yang, D. Choi, S. Kerisit, K.M. Rosso, D. Wang, J. Zhang, G. Graff, J. Liu, J. Power Sources 192 (2009) 588.
[10] A. Du Pasquier, C.C. Huang, T. Spitler, J. Power Sources 186 (2009) 508.
[11] T.-F. Yi, L.-J. Jiang, J. Shu, C.-B. Yue, R.-S. Zhu, H.-B. Qiao, J. Phys. Chem. Solids 71 (2010) 1236.
[12] A.S. Prakash, P. Manikandan, K. Ramesha, M. Sathiya, J.-M. Tarascon, A.K. Shukla, Chem. Mater. 22 (2010) 2857.
[13] D. Bresser, E. Paillard, M. Copley, P. Bishop, M. Winter, S. Passerini, J. Power Sources 219 (2012) 217.
[14] S.-T. Myung, N. Takahashi, S. Komaba, C.S. Yoon, Y.-K. Sun, K. Amine, H. Yashiro, Adv. Funct. Mater. 21 (2011) 3231.
[15] C. Jiang, J. Zhang, J. Mater. Sci. Technol. 29 (2013) 97.
[16] T. Froeschl, U. Hormann, P. Kubiak, G. Kucerova, M. Pfanzelt, C.K. Weiss, R.J. Behm, N. Husing, U. Kaiser, K. Landfester, M. Wohlfahrt-Mehrens, Chem. Soc. Rev. 41 (2012) 5313.
[17] A.L. Linsebigler, G. Lu, J.T. Yates, Chem. Rev. 95 (1995) 735.
[18] U. Bach, D. Lupo, P. Comte, J.E. Moser, F. Weissortel, J. Salbeck, H. Spreitzer, M. Gratzel, Nature 395 (1998) 583.
[19] M. Grätzel, J. Photochem. Photobiol. C Photochem. Rev. 4 (2003) 145.
[20] B. Zachau-Christiansen, K. West, T. Jacobsen, S. Atlung, Solid State Ionics 28–30 (1988) 1176.
[21] T. Ohzuku, T. Kodama, T. Hirai, J. Power Sources 14 (1985) 153.
[22] L. Kavan, M. Grätzel, S.E. Gilbert, C. Klemenz, H.J. Scheel, J. Am. Chem. Soc. 118 (1996) 6716.
[23] M. Wagemaker, D. Lützenkirchen-Hecht, A.A. van Well, R. Frahm, J. Phys. Chem. B 108 (2004) 12456.
[24] M. Wagemaker, W.J.H. Borghols, F.M. Mulder, J. Am. Chem. Soc. 129 (2007) 4323.
[25] G. Sudant, E. Baudrin, D. Larcher, J.-M. Tarascon, J. Mater. Chem. 15 (2005) 1263.
[26] D. Bresser, E. Paillard, E. Binetti, S. Krueger, M. Striccoli, M. Winter, S. Passerini, J. Power Sources 206 (2012) 301.
[27] L.J. Hardwick, M. Holzapfel, P. Novák, L. Dupont, E. Baudrin, Electrochim. Acta 52 (2007) 5357.
[28] A.S. Aricò, P. Bruce, B. Scrosati, J.M. Tarascon, W. van Schalkwijk, Nat. Mater. 4 (2005) 366.
[29] P.G. Bruce, B. Scrosati, J.-M. Tarascon, Angew. Chem. Int. Ed. 47 (2008) 2930.
[30] J. Moskon, R. Dominko, R. Cerc-Korosec, M. Gaberscek, J. Jamnik, J. Power Sources 174 (2007) 683.
[31] D. Wang, D. Choi, J. Li, Z. Yang, Z. Nie, R. Kou, D. Hu, C. Wang, L.V. Saraf, J. Zhang, I.A. Aksay, J. Liu, ACS Nano 3 (2009) 907.
[32] L.J. Fu, L.C. Yang, Y. Shi, B. Wang, Y.P. Wu, Microporous Mesoporous Mater. 117 (2009) 515.
[33] S.K. Das, M. Patel, A.J. Bhattacharyya, ACS Appl. Mater. Interfaces 2 (2010) 2091.
[34] F.-F. Cao, X.-L. Wu, S. Xin, Y.-G. Guo, L.-J. Wan, J. Phys. Chem. C 114 (2010) 10308.
[35] V.G. Pol, S.-H. Kang, J.M. Calderon-Moreno, C.S. Johnson, M.M. Thackeray, J. Power Sources 195 (2010) 5039.
[36] G.-N. Zhu, C.-X. Wang, Y.-Y. Xia, J. Electrochem. Soc. 158 (2011) A102.
[37] J. Wang, X. Sun, Energy Environ. Sci. 5 (2012) 5163.
[38] B. Oschmann, D. Bresser, M.N. Tahir, K. Fischer, W. Tremel, S. Passerini, R. Zentel, Macromol. Rapid Commun. (2013), http://dx.doi.org/10.1002/marc201300531.
[39] C.-T. Dinh, T.-D. Nguyen, F. Kleitz, T.-O. Do, ACS Nano 3 (2009) 3737.
[40] A. Dong, X. Ye, J. Chen, Y. Kang, T. Gordon, J.M. Kikkawa, C.B. Murray, J. Am. Chem. Soc. 133 (2010) 998.
[41] M.R. Ranade, A. Navrotsky, H.Z. Zhang, J.F. Banfield, S.H. Elder, A. Zaban, P.H. Borse, S.K. Kulkarni, G.S. Doran, H.J. Whitfield, Proc. Natl. Acad. Sci. U. S. A. 99 (2002) 6476.
[42] A.A. Levchenko, G. Li, J. Boerio-Goates, B.F. Woodfield, A. Navrotsky, Chem. Mater. 18 (2006) 6324.
[43] Y. Chen, K.S. Kang, K.H. Yoo, N. Jyoti, J. Kim, J. Phys. Chem. C 113 (2009) 19753.
[44] D.J. Reidy, J.D. Holmes, M.A. Morris, J. Eur. Ceram. Soc. 26 (2006) 1527.
[45] R. Baddour-Hadjean, S. Bach, M. Smirnov, J.-P. Pereira-Ramos, J. Raman Spectrosc. 35 (2004) 577.
[46] D.S. Knight, W.B. White, J. Mater. Res. 4 (1989) 385.
[47] R. Baddour-Hadjean, J.-P. Pereira-Ramos, Chem. Rev. 110 (2010) 1278.
[48] M. Mancini, F. Nobili, R. Tossici, M. Wohlfahrt-Mehrens, R. Marassi, J. Power Sources 196 (2011) 9665.
[49] A. Moretti, G.-T. Kim, D. Bresser, K. Renger, E. Paillard, R. Marassi, M. Winter, S. Passerini, J. Power Sources 221 (2013) 419.
[50] D.W. Murphy, R.J. Cava, S.M. Zahurak, A. Santoro, Solid State Ionics 9–10 (Part 1) (1983) 413.
[51] R.J. Cava, D.W. Murphy, S. Zahurak, A. Santoro, R.S. Roth, J. Solid State Chem. 53 (1984) 64.
[52] M. Wagemaker, R. van de Krol, A.P.M. Kentgens, A.A. van Well, F.M. Mulder, J. Am. Chem. Soc. 123 (2001) 11454.
[53] W.J.H. Borghols, D. Lutzenkirchen-Hecht, U. Haake, E.R.H. van Eck, F.M. Mulder, M. Wagemaker, Phys. Chem. Chem. Phys. 11 (2009) 5742.
[54] U. Lafont, D. Carta, G. Mountjoy, A.V. Chadwick, E.M. Kelder, J. Phys. Chem. C 114 (2010) 1372.
[55] A.A. Belak, Y. Wang, A. Van Der Ven, Chem. Mater. 24 (2012) 2894.
[56] J.-Y. Shin, D. Samuelis, J. Maier, Adv. Funct. Mater. 21 (2011) 3464.
[57] J. Wang, J. Polleux, J. Lim, B. Dunn, J. Phys. Chem. C 111 (2007) 14925.
[58] R. van de Krol, A. Goossens, J. Schoonman, J. Phys. Chem. B 103 (1999) 7151.
[59] C. Jiang, M. Wei, Z. Qi, T. Kudo, I. Honma, H. Zhou, J. Power Sources 166 (2007) 239.
[60] J.W. Kang, D.H. Kim, V. Mathew, J.S. Lim, J.H. Gim, J. Kim, J. Electrochem. Soc. 158 (2011) A59.
[61] R.A. Huggins, J. Power Sources 81–82 (1999) 13.
[62] K. Saravanan, K. Ananthanarayanan, P. Balaya, Energy Environ. Sci. 3 (2010) 939.
[63] L. Kavan, M. Kalbáč, M. Zukalová, I. Exnar, V. Lorenzen, R. Nesper, M. Graetzel, Chem. Mater. 16 (2004) 477.
[64] B. Laskova, M. Zukalova, A. Zukal, M. Bousa, L. Kavan, J. Power Sources 246 (2014) 103.
[65] M. Zukalová, M. Kalbáč, L. Kavan, I. Exnar, M. Graetzel, Chem. Mater. 17 (2005) 1248.
[66] T. Kogure, T. Umezawa, Y. Kotani, A. Matsuda, M. Tatsumisago, T. Minami, J. Am. Ceram. Soc. 82 (1999) 3248.
[67] B.M. Rabatic, N.M. Dimitrijevic, R.E. Cook, Z.V. Saponjic, T. Rajh, Adv. Mater. 18 (2006) 1033.
[68] R. Hengerer, L. Kavan, P. Krtil, M. Grätzel, J. Electrochem. Soc. 147 (2000) 1467.
[69] C.H. Sun, X.H. Yang, J.S. Chen, Z. Li, X.W. Lou, C. Li, S.C. Smith, G.Q. (Max) Lu, H.G. Yang, Chem. Commun. 46 (2010) 6129.
[70] S. Lunell, A. Stashans, L. Ojamäe, H. Lindström, A. Hagfeldt, J. Am. Chem. Soc. 119 (1997) 7374.